Title
Electroencephalography (EEG): Neurophysics, Experimental Methods, and Signal Processing

ISBN
9781482220971

Authors
Nunez, Michael D
Nunez, Paul L
Srinivasan, Ramesh

Publication Date
2016-11-14

APA Citation (BibTeX last page):

Nunez, M. D., Nunez, P. L., & Srinivasan, R. (2016). Electroencephalography (EEG): neurophysics, experimental methods, and signal processing. In Ombao, H., Linquist, M., Thompson, W. & Aston, J. (Eds.) *Handbook of Neuroimaging Data Analysis* (pp. 175-197), Chapman & Hall/CRC. Advance online publication. doi: 10.13140/rg.2.2.12706.63687

Electroencephalography (EEG): neurophysics, experimental methods, and signal processing

Michael D. Nunez[1], Paul L. Nunez[2], and Ramesh Srinivasan[1,3]

Department of Cognitive Sciences, University of California, Irvine[1]

Cognitive Dissonance, LLC[2]

Department of Biomedical Engineering, University of California, Irvine[3]

Address for Correspondence

Ramesh Srinivasan, r.srinivasan@uci.edu

Acknowledgments: This work was supported by a grant from the NIH 2R01-MH68004

1. Introduction

Electroencephalography (EEG) is the measurement of the electric potentials on the scalp surface generated (in part) by neural activity originating from the brain. The sensitivity of EEG to changes in brain activity on such a millisecond time scale is the major advantage of EEG over other brain imaging modalities such as functional magnetic resonance imaging (fMRI) or near-infrared spectroscopy (NIRS) that operate on time scales in the seconds to minutes range. Over the past 100 years, neuroscientists and clinical neurologists have made use of EEG to obtain insight into cognitive or clinical disease state by applying a variety of signal processing and statistical analyses to EEG time series. More recently there has been growing interest in making use of statistical modeling of EEG signals to directly control physical devices in Brain-Computer Interfaces. In this chapter we provide an introduction to EEG generation and measurement as well as the experimental designs that optimize information acquired by EEG.

EEG has statistical properties that vary over time and space. That is, we assume the data recorded are observations of a spatio-temporal stochastic process. The starting point of most EEG analysis is to consider the properties of the time series at each electrode, such as spectral power, in relation to sensory stimulation, cognitive processing, or clinical disease state. EEG power is typically split up into bands which correspond to different spectral peaks that relate to behavior or cognitive state. These bands are typically defined as the delta (1-4 Hz), theta (4-8 Hz), alpha (8-13 Hz), beta (13-20 Hz), and gamma (>20 Hz) bands and can have high-power over spatially distinct regions on the scalp, as shown by an EEG recording of a subject at rest in Figure 1. Because this EEG was recorded using a *high-density*, 128 electrode net, the topographic scalp maps could be found by interpolating values between electrodes. Modern EEG systems typically use a large number of electrodes (ranging from 64 to 256) to provide coverage over most of the scalp, enabling the analyses of *spatial* properties of EEG, such as correlation or coherence between electrode sites.

In this chapter we first review physical properties of EEG recordings, in order to model the relationship between potentials on the scalp and current sources in the brain. Models of volume conduction of current passing through the head imply that EEG signals

are strongly influenced by the synchronization of neural current sources; EEG is as much a measure of neural synchrony as neural activity. We then introduce issues in EEG recording and preprocessing, with particular emphasis on the problem of artifacts. The last two sections consider the types of EEG analyses appropriate for different experimental designs.

2. The neurophysics of EEG

Scalp potentials are believed generated by *millisecond-scale modulations* of synaptic current sources at neuron surfaces (Lopes da Silva and Storm van Leeuwen 1978; Nunez 1981, 1995; 2000a,b; Lopes da Silva 1999), while single neuron firings of *action potentials* are mainly absent in scalp activity due to other, inactive neurons contributing to low-pass temporal filtering (Nunez and Srinivasan, 2006; Buzsáki, 2006). Action potential time scales are typically on the order of less than 1 ms, while synaptic potentials occur on the order of 10 ms or more—a time scale more consistent with the oscillations observed in EEG. Any patch of cortex 3-5 mm in diameter and traversing all cortical layers contains ~ 10^6 neurons and perhaps 10^{10} synapses (Nunez, 1995). Excitatory and inhibitory synapses inject current into the cell bodies and induce extracellular potentials (via return currents) of opposite polarity. These extracellular currents yield the electrical potentials recorded on the scalp with EEG.

When measurement of the potential is taken at "large" distance away from the source region, a complex current distribution in a small volume can be approximated by a dipole or more accurately, *a dipole moment per unit volume* (Nunez and Srinivasan, 2006). The (current) dipole moment per unit volume is an intermediate scale vector function based on the distribution of positive and negative micro-current sources in each local tissue mass, typically applied to cortical columns. The dipole approximation to cortical current sources provides a basis for realistic models of EEG signals. A "large" distance in this case is at least 3 or 4 times the distance between the effective poles of the dipole. In the context of EEG recording, the dipole approximation appears valid for potentials in superficial cortical tissue with a maximum extent in any dimension of roughly 0.5 cm or less. This is because superficial gyral surfaces are located at roughly

1.5-2 cm from scalp electrodes, separated by a thin layer of passive tissue, including cerebrospinal fluid (CSF), skull, and scalp.

Thus, the current sources in the brain that generate EEG can be modeled in terms of dipole moment per unit volume $\boldsymbol{P}(\boldsymbol{r}', t)$ for any time t where the location vector $\boldsymbol{r}'$ spans the volume of the brain. For convenience of this discussion, the brain volume may be parceled into N small tissue masses of volume ΔV (e.g., 3 mm x 3mm x 3mm), each producing its vector dipole moment, such that, in an adult brain, N ~ 10^5 to 10^6. The strength and orientation of each vector depends on the distribution and synchrony of excitatory and inhibitory post-synaptic potentials within the tissue mass (Nunez and Srinivasan, 2006). The potential on the scalp surface can then be expressed as a weighted sum (or integral) of contributions from all these sources. In most models, each volume element $V(\boldsymbol{r}')$ is located only within the superficial cortex since current sources in deeper tissues, such as the thalamus or midbrain typically contribute very little to scalp potentials (Nunez and Srinivasan, 2006). Thus, the volume integral may be reduced to a surface integral over the folded cortical surface

$$\Phi_S(\mathbf{r},t) = \int_{B'} G_H(\mathbf{r},\mathbf{r}')\mathbf{P}(\mathbf{r}',t)dV(\mathbf{r}') \qquad (1)$$

The weighting term G_H is the Green's function for volume conduction of current passing through the tissues of the head. It depends on both the location of source $\boldsymbol{r}'$ and the location of the scalp electrode $\boldsymbol{r}$. The Green's function can be thought of as the *impulse response function* between sources and surface locations and contains all geometric and conductive information about the head as a volume conductor. G_H will be larger for superficial sources in the visible gyral crowns of the cortex than for deeper sources, such as in the sulcal walls (folded surfaces) or sources on the mesial (underside) of the brain.

Any model of head volume conduction, i.e., any form of the function G_H, is only an approximation. Magnetic Resonance Imaging (MRI) can provide geometric information by imaging the boundaries between tissue compartments with different electrical conductivity (the inverse of resistivity). Numerical methods such as the Boundary Element Method (BEM) or Finite Element Methods (FEM) may then be used

to estimate G_H, by employing MRI to determine tissue boundaries as shown in the examples in Figure 2 (b and c). However, the geometric model obtained from MRI is still only approximate due to limits in spatial resolution (typically 2-5 mm). And even if we were able to obtain perfect geometric information, the head model would still only be approximate due to the substantial uncertainty in our knowledge of tissue conductivities (Nunez and Srinivasan, 2006).

The poor conductivity of the skull is the feature that most strongly determines volume conduction in the head. Estimates of the conductivity of the skull vary widely depending on whether the estimate is in-vivo or in-vitro and differ between skull samples from different regions of the head. Skull itself is composed of three layers of different conductivity which vary in thickness across the head (Nunez and Srinivasan, 2006) and are not easily measured with MRI (Srinivasan, 2006).

Despite these uncertainties in the geometry and conductivity of the head, the gross features of volume conduction are captured by any model that includes a poorly conducting skull layer in between conductive soft tissue. A simple estimate of G_H can be provided by models which consist of three concentric spherical shells (brain, skull, and scalp) or four shells when including a CSF layer as shown in Figure 2a, such that these models have been useful in a number of simulation studies (Nunez et al., 1994; Srinivasan et al., 1998; Nunez and Srinivasan, 2006). These models also have the advantage of easy checking of computational accuracy as analytic solutions for these models have been obtained (Nunez and Srinivasan, 2006). The following gross features of head volume conduction are captured by this model: (1) the poor conductivity of the skull results in very little current entering the skull from the brain. (2) Current is expected to mostly flow radially through the skull into the scalp as current follows the path of least resistance. Exceptions are holes in the skull like the nasal passages. (3) All of the current is contained in the scalp, as no current can enter the surrounding air. (4) Very little current is expected to enter the body because of the high resistance of the neck, such that the head can be considered a closed object to first approximation. In all models that contain these essential features, the tangential spread of current within the scalp leads to the "smearing" of the scalp potential, i.e., low-pass spatial filtering, resulting in the low spatial resolution of EEG as compared to direct recordings on the brain surface. Thus this

model captures the fact that EEG is a direct measurement of the current flowing in the scalp.

There is considerable interest in the EEG literature in developing methods to estimate the current source distribution in the brain $\boldsymbol{P(r', t)}$ from the EEG recording and a volume conduction model of the head. However, this *inverse problem is ill-posed*; given the potential distribution on the surface of the scalp, it is not possible to estimate the source distribution without additional assumptions (Nunez and Srinivasan, 2006). That is, for any given G_H estimate and true scalp potential $\Phi_S(\boldsymbol{r}, t)$ there are a large number of solutions for $\boldsymbol{P(r', t)}$. Although in some cases, for example an epileptic focus in the cortex, it may be reasonable to assume a single isolated source $\boldsymbol{P}(\boldsymbol{r}', t)$ in order to find a solution. Another popular approach that is widely adopted is to use Tikhanov regularization to obtain a minimum L^2 norm estimate of $\boldsymbol{P}(\boldsymbol{r}', t)$ (Hauk, 2004). While this approach is mathematically tractable, there is no apparent theoretical reason why neuroscientists should seek solutions with a minimum L^2 norm. More recently, methods based on Bayesian inference have been developed which have the advantage of making assumptions explicit. These methods allow for the possibility of model validation and allow for comparisons between models based on different assumptions (Baillet and Garnero, 1997; Wipf and Nagarajan, 2009). They also allow for the use of prior information, for example by making use of fMRI information to influence the source solutions (Henson et al., 2010).

3. Synchronization and EEG

The magnitude of the scalp potential recorded with EEG can change for several reasons related to source synchronization. The large changes in scalp amplitude that occur when brain state changes are believed to be due mostly to distributed synchronization changes. That is, large-scale synchronization increases (or decreases) over cm scales in the tangential direction across the cortex will cause increases (or decreases) in scalp potential if there are no other changes. With this knowledge, EEG scientists and clinicians have adopted the label *desynchronization* to indicate large amplitude reductions (Pfurtscheller and Lopes da Silva 1999). Although, at any one

location $\boldsymbol{r}'$ in the brain, small-scale changes in synaptic source synchronization will *also* change the magnitude (or source strength) of $\boldsymbol{P}(\boldsymbol{r}', t)$ (Nunez and Srinivasan, 2006), we will concentrate in this section on large-scale synchronization that does not change the magnitude of each individual dipole moment $\boldsymbol{P}(\boldsymbol{r}', t)$. Instead, we will show that large-scale changes across different locations $\boldsymbol{r}'$ cause the scalp potential in Eq. 1 to decrease; this is because the integral approaches zero as more random positive and negative dipole moments $\boldsymbol{P}(\boldsymbol{r}', t)$ at different cortical locations $\boldsymbol{r}'$ cancel. However if multiple locations $\boldsymbol{r}'$ have similar dipole moments per unit volume $\boldsymbol{P}(\boldsymbol{r}', t)$ then synchronization occurs which leads to larger observed scalp potentials.

We expect that the source of any EEG signal will never simply correspond to source activity in only one of the volume elements. Because neurons are highly interconnected, most EEG signals are generated by sources with spatial extent, i.e., patches of cortical tissue. Figure 3 shows examples of scalp potentials simulated in a concentric spheres volume conduction model due to a single dipole (a; corresponding to a patch of diameter < 3 mm) as well as dipole layers of diameter ranging from 3-5 cm (Fig. 3c, 3e, & 3g). For simplicity, we only make use of radial dipole sources in this example as similar effects could be found with dipole layers of arbitrary orientation. Each dipole layer is composed of dipole sources with time series that are constructed by adding a 6 Hz sinusoid of fixed amplitude A=15 to a Gaussian random processes with mean μ=0 and standard deviation σ=150. *The 6 Hz components are synchronized across the dipole layers, whereas all other frequencies will have random phases*. Each source signal is an independent random time series representing the potential across the cortical surface given by the dipole layer. The source time series of a single dipole source (i.e. the dipole layer of very small size) is plotted in Figure 3a. The magnitude of the 6 Hz sinusoid is only 1% of the total variance of each dipole source, and the sinusoid is not observable in the dipole time series. Figure 3b shows the estimated potential measured at an electrode on the scalp directly above the center of a dipole layer of diameter 3 cm, based on a four concentric spheres model of the head (see Figure 3 caption for details of the head model). The time series exhibits a smoother appearance compared to the source time series. And as the diameter of the dipole layer is increased from 3 to 4 to 5 cm (i.e. increasing

synchrony), the calculated surface potential becomes more obviously sinusoidal (Fig. 3c through 3h).

Clearly, spatial synchrony is a least as important as the strength of the source in the generation of scalp potentials. Most (99%) of the source activity in these examples is uncorrelated Gaussian noise across the dipoles in a patch of width 5 cm. Yet, the scalp potential will appear smooth and periodic reflecting mostly relatively small magnitude (1% of) source activity that is synchronous across all sources in the dipole layer. The effect of volume conduction is to sum the source activity at the scalp electrode, so the asynchronous source time series contribute minimally due to noise cancellation. The synchronized 6 Hz signal is emphasized and the scalp potential is remarkably sensitive to the size of the dipole layer.

We have previously quantified this effect as spatial filtering by volume conduction (Srinivasan et al, 1998; Nunez and Srinivasan, 2006; Srinivasan et al, 2007). *One important implication is that spatial filtering by volume conduction can generally be expected to filter the temporal structure of source activity in the scalp EEG.* If sources with different time series take place in dipole layers of different sizes, EEG favors signals that are synchronized broadly over the cortical surface. The magnitude of any scalp EEG signal is determined not only by the source strength but also by spatial properties of the source such as its size and synchrony. Thus, we anticipate that EEG recorded within the brain (known as electrocorticography or ECoG) will have quite different properties than EEG recorded on the scalp. Neither signal is a more accurate representation of brain activity; instead they emphasize different spatial scales of synchronization in the brain.

4. Recording EEG

Every EEG recording involves at least 3 electrodes, two measurement electrodes and a ground electrode. Brain sources $\boldsymbol{P}(\boldsymbol{r}, t)$ (current dipole moments per unit volume) and biological artifacts generate the majority of scalp potential differences $V_2(t) - V_1(t)$. Environmental electric and magnetic fields also contribute to the measured scalp potential due mostly to capacitive coupling of body and electrode leads to power line fields. However, the amplifier ground electrode placed on the scalp, nose, or neck

provides a reference voltage to the amplifier to prevent amplifier drift and facilitate better common mode rejection by serving as a reference for the differential amplifier (Nunez and Srinivasan, 2006).

Typically one electrode is singled out as the "reference electrode"; the remaining electrodes are characterized as "recording" electrodes. But electrode pairs are always required to measure scalp potentials because such recording depends on current passing through a measuring circuit (Nunez and Srinivasan, 2006). There are no monopolar recordings in EEG; all recordings are bipolar. Every EEG recording depends on the location of both recording and "reference" electrodes. Therefore any particular choice of reference placement offers possible advantages and disadvantages depending on actual source locations.

But, in general, we do not know the location of the sources prior to recording EEG, so no ideal reference location is likely to be found in advance. Reference strategies have often been adopted in EEG laboratories without a clear understanding of the attendant biases imposed on the recording. The linked-ears or linked-mastoids reference, a historically popular reference choice with cognitive scientists, is one such idea with minimal theoretical justification, but nevertheless persists in a number of laboratories. In EEG, *we generally measure potential differences between two locations on the head, and these differences depend on both electrode locations*, as well as on all brain generator configurations and locations.

In most EEG practice, the potentials at all the other electrode sites (typically 32-256) are recorded with respect to the reference electrode. The position of these electrodes varies considerably across laboratories. Standard electrode placement strategies make use of the 10-20, 10-10, and 10-5 electrode placement systems (Oostenveld and Praamstra, 2001). These systems are widely but not universally used. For larger numbers of channels (> 64), other electrode placement systems have been developed in order to obtain more uniform sampling of scalp potential, which is advantageous for source localization and high resolution EEG methods (Tucker, 1993). The reference point is largely arbitrary; it is special only because we choose to record potential differences with respect to one fixed location. But we do have the option of changing the effective reference to another recording site further down the processing chain by simple

subtraction.

The average reference (also called common average reference or global average reference) has become commonplace in EEG studies and has some theoretical justification (Bertrand et al. 1985). When recording from N electrodes located at scalp locations r_n, $n = 1, 2,\ldots, N$, the measured potentials $V(r_n)$ are related to the true scalp potential $\Phi(r_n)$ (measured with respect to "infinity") by

$$V(r_n) = \Phi(r_n) - \Phi(r_R) \qquad (2)$$

where r_n is the position of the nth electrode and r_R is the reference electrode site. If we sum over all N electrodes, the potential with respect to infinity at the reference site can be written in terms of the scalp potentials as

$$\Phi(r_R) = \frac{1}{N}\left(\sum_{n=1}^{N} \Phi(r_n) - \sum_{n=1}^{N} V(r_n) \right) \qquad (3)$$

The first term on the right side of Eq. 3 is the average of the scalp surface potential at all recording sites. Theoretically, this term vanishes if the mean of the potentials approximates a surface integral over a closed surface containing all current within the volume. Only minimal current flows from the head through the neck even with reference electrode placed on the body, so a reasonable approximation considers the head to be a closed volume that confines all current. The surface integral of the potential over a volume conductor containing dipole sources must be zero as a consequence of current conservation (Bertrand et al., 1985). If we make this assumption, the reference potential can be estimated by the second term on the right side of Eq. 3; that is, by averaging the measured potentials at all electrodes and changing the sign of this average. This reference potential (i.e. the average across electrodes) can thus be added to each measurement $V(r_n)$, thereby estimating the reference-free potential $\Phi(r_n)$ (potential with respect to "infinity") at each location r_n.

However since we cannot measure the potentials on a closed surface surrounding the brain, the first term on the right side of Eq. 3 will not generally vanish. The distribution of potential on the underside of the head (within the neck region) cannot be

measured. Furthermore, the average potential for any group of electrode positions, given by the second term on the right side of Eq 3, is only an approximation of the surface integral. For example, the average potential is expected to be a very poor approximation if applied with the standard 10-20 electrode system with 21 electrodes. As the number of electrodes increases to 64 or more, the error in the approximation is expected to decrease. Thus, like any other choice of reference, the average reference provides biased estimates of reference-independent potentials. Nevertheless, when used in studies with large numbers of electrodes (say 128 or more), we have found that the average reference performs reasonably well as an estimate of reference independent potentials (Srinivasan et al., 1998).

5. Preprocessing EEG

Measured EEG signals have been amplified and filtered by analog circuits to remove both low and high frequency noise as well as power at frequencies greater than the Nyquist limit, established by the sampling rate of the analog to digital converter (ADC). The discrete sampling of continuous signals is a well-characterized problem in time series acquisition and analysis (Bendat and Piersol, 2001). The central concept is the Nyquist criterion: $f_{dig} > 2f_{max}$ where f_{dig} is the digitization rate or sampling rate and f_{max} is the highest frequency present in the time series. For instance, if the highest frequency in a signal is 20 Hz (cycles/sec), a minimum sampling rate of 40 Hz (one sample every 25 ms) is required to record the signal discretely without aliasing. Aliasing is the misrepresentation of a high-frequency signal as a low-frequency signal because the sampling rate used during analog-to-digital conversion is lower than the Nyquist limit. If a time series has been aliased by under-sampling, no digital signal processing method can undo the aliasing because the necessary information for this procedure has been lost. In conventional EEG practice, a sampling rate is selected and the aliasing error is avoided by applying (in hardware) a low-pass filter to the analog signal that eliminates power at frequencies greater than the maximum frequency determined by the Nyquist limit. The low-pass filter is typically applied with a cut-off frequency 2.5 times smaller than the sampling rate. This more restrictive limit, known as the Engineer's Nyquist criterion,

accounts for the possibility of phase-locking between the sampling and high-frequency components of the signal (Bendat and Piersol, 2001). The analog signal from each channel is sampled at perhaps 200 to 1000 times per second, assigned numbers proportional to instantaneous amplitude (digitized), and converted from ADC units to volts. These samples can then be stored digitally in conventional EEG practice or further processed online (e.g., using an FFT) in certain clinical or BCI applications.

The choice of filter settings requires some care. Clearly a low-pass filter must be set to insure removal of power at the very high frequencies determined by the Nyquist criterion. However, severe low pass filtering runs the risk of removing obvious muscle artifact at high frequencies (which would indicate time segments of data that potentially needs to be discarded), while passing muscle artifact at frequencies overlapping with EEG that can be easily mistaken for EEG (Fisch, 1999). For example, imagine using an analog filter to remove most power at frequencies greater than 20 Hz, thereby obtaining a much cleaner looking signal. However, the remaining signal might well contain significant muscle artifact in roughly the 15-30 Hz range (beta band), which is much harder to identify without the information at higher frequencies. Such subtle artifact could substantially reduce the signal to noise ratio in the beta band. Some EEG systems have notch filters to remove power line interference (60 Hz in the Americas; 50 Hz in Europe, Australia, and Asia). However, the presence of power line noise in the recorded EEG signal is an easy way to detect electrodes that develop high contact impedances (or come off entirely) during the recording. If EEG processing and analysis is based on FFT or other spectral analysis methods, the presence of moderate 60 Hz noise will have no practical effect on results at lower frequencies which contain most of the EEG information.

6. Artifact removal

A substantial portion of the electrical signals recorded from EEG systems originate from outside the brain (Nunez and Srinivasan, 2006; Whitham et al., 2007). For example, in some areas on the head, close to the ears, eyes, and neck, we expect electrical signals originating in the cortex to have magnitude as much as 200 times lower than

electrical signals from muscle activity (Fitzgibbon et al., 2015). Furthermore, movement of the head will generate artifacts over a large number of electrodes. Potentials generated from sources other than cortical activity are dubbed *artifact*, and a major challenge in EEG analysis is to detect these signals and remove them from EEG recordings.

Artifact can either be biological in nature, such as muscle activity, or due to environmental factors such as electric fields caused by the common AC standard and temporary potential shifts due to movement. Biological artifact is typically caused by electrical potentials generated by muscle activity. The recording of muscle activity is known as electromyography (EMG) and typically originates from the eyes, face, and neck, but also from muscles all over the body (Whitham et al., 2007). Another source of common artifact is the rhythmic beating of arteries in the temples or neck and potentials from distant but large muscles in the heart (electrocardiography or EKG). Transient muscle artifact can be due to head movements, eye blinks, lateral eye-movement, or jaw clenching; all of which may display different spatio-temporal patterns of potentials on the scalp.

In order to better draw inference about brain activity, multiple procedures have been developed to reduce the contribution of artifact in EEG recordings. Ocular artifact such as eye blinks and lateral eye movements can be automatically removed using regression methods (Gratton et al., 1983). In a typical ocular regression method, electrodes are placed near the eyes to record electrooculographic (EOG) signals, potentials generated by musculature associated with the eyes. The effect of these EOG signals on the other EEG channels is then estimated with linear regression. The total influence of the EOG signals on the EEG is then removed by subtracting the product of the EOG signals and the regression coefficient estimates (Schlögl et al., 2007).

Independent Component Analysis (ICA; Bell & Sejnowski, 1995) has become an important tool for identifying and removing artifact. Independent component analysis (ICA) refers to a class of blind source-separation algorithms used to decompose linear mixtures of data. For example, some ICA algorithms find linear mixtures of variables that are maximally non-Gaussian by searching for mixtures with either minimum mutual information or maximum kurtosis (Makeig et al. 1996; Jung et al., 1998). In practice these methods often yield non-normal mixtures that have distributions with outliers. The

two most widely used algorithms in the EEG literature are the FastICA (Hyvärinen & Oja, 1997) and InfoMax ICA (Bell & Sejnowski, 1995; Delorme & Makeig, 2002).

ICA assumes that there is a linear mixture of the EEG data *V* (a channels *c* by time *t* matrix) such that the independent components *M* (a component *k* by time *t* matrix) are given by $M = W^{-1}V$ where W^{-1} is the matrix consisting of *k* by *c* weights. Some of the resulting components have been shown to well represent some specific types of artifact (Delorme et al. 2007). The components evaluated to reflect artifact can then be removed from the data by inverting the equation using a reduced matrix W_L to remove the artifact components.

There are two caveats with this approach. First, the identification of the artifact component is inherently a subjective judgement. Some artifact sources are easy to identify such as eye blinks, eye movements, and temporary electrical discontinuities (perhaps due to a reference electrode or ground electrode displacement during head movement). But artifacts due to muscle are far more subtle. Second, the effect of reducing the number of sources in M is to reduce the rank of the data matrix, which potentially influences further analysis by reducing the amount of possible EEG mixtures.

To perform an ICA based artifact removal procedure, the continuous recording is first split into 1-3 second epochs, usually based on the trial structure of the experiment in cognitive experiments. Epochs that obviously contain artifact rather than EEG, usually due to gross movements by the subject, can then be rejected by visual inspection, or by examining trials with high variance compared to other trials. Not removing this one-off data hinders the ability of the ICA algorithm to isolate typical artifacts such as eye blinks. After this “precleaning” step, an algorithm is run with the EEG data as input to obtain an ICA decomposition.

Typical graphical representations of Independent Components (ICs) are topographic maps of the inverse weights, component spectra, and component time series or average component time series across epochs. Figure 4 provides typical graphical representations of the 12 components that describe the most variance in a subject's EEG data using InfoMax ICA. The EEG was collected from a subject at rest who fixated on a cross on a monitor for 42 seconds. Due to properties of the weight matrix *W* (columns represented as the circular head plots in Figure 4 corresponding to each component), the

component spectra and the component time series, we identified 4 components that could be indicative of artifact. Component 1 (IC1) most likely captures the electrical potentials due to eye blinks. Indicative of eye blinks, the channel weights indicate that all the component information is located near the eyes. The power spectrum has one peak in a low frequency band because the time series has high amplitude waveforms located sparsely in time (which occur once per blink). IC12 is probably muscle artifact, perhaps due to facial tension. It contributes to the EEG recording mainly at peripheral electrodes, and its spectrum has high power at high frequencies and low power at typical resting EEG frequencies (such as alpha rhythm, around 10 Hz). Furthermore, the topography's spatial frequency is too high (i.e. too focal) as this spatial frequency is near impossible for EEG to obtain due to the properties of head volume conduction which acts as a low-pass spatial filter. Similarly, IC6 captures data that cannot be due to brain activity because its weight is only at one electrode and the power spectrum exhibits a 1/f frequency falloff (a property of electrical *"pink"* noise). As indicated by its time course, this component is probably a mix of a temporary electrical discontinuity at about 6 seconds and a horizontal eye movement at about 12 seconds. IC7 is similar in its properties to IC6 and captures only a temporary electrical discontinuity at 41 seconds. The rest of the ICs most likely reflect cortical electrical activity or mixtures of cortical electrical activity and muscle artifact. These ICs contain peaks in alpha (8-13 Hz) and/or beta frequency bands (13-20 Hz) and have lower spatial frequency distributions typical of EEG.

We recommend keeping EEG and artifact mixtures in the data unless very specific properties of the EEG are of interest a priori. There is empirical evidence to suggest that ICA algorithms do not isolate many types of muscle artifact, especially task related artifact, and thus rejecting ICs that do not clearly represent artifact becomes very subjective (Shackman et al., 2009). Furthermore, the efficacy of ICA to reduce *all* EMG artifact remains controversial at best (Olbrich et al., 2011; McMenamin et al., 2011). However if one must analyze a dataset that has a large quantity of muscle artifact, there may be a few indicators of EEG data that do not originate in the brain. For instance, an IC representing EEG or an EEG-EMG mixture may have a constant distribution of sample variances over all trials if the subject is in the same cognitive state and is doing the same

task. In contrast, irregular EMG components will typically only have large variances on only a few trials.

In order to reduce subjectivity of the artifact independent component (IC) removal process and reduce the time demand on performing artifact removal, some progress has been made on automatic rejection of artifact components. ADJUST is an algorithm that uses properties of the components such as spatial weight distributions on the scalp, variance, and kurtosis of the components' potentials to automatically label components as eye blinks, vertical eye movements, horizontal eye movies, or generic potential discontinuities so that they can be subtracted from the recording (Mognon et al., 2011)

No known modern artifact correction technique is perfect for muscle artifact removal, and no EEG recording is completely immune to muscle artifact (Whitham et al., 2007). This is particularly the case for the neck and face muscle variety; thus, good recording and analysis practices are still the best approach for reducing artifact in EEG recordings. Subjects should be told to remain still and minimize jaw clenching, and the electrode cap or net should be positioned tightly (but comfortably) on the subject. Muscle artifact exhibits broadband frequency spectra with substantial relative power above 15 Hz; therefore analyses of the delta (1-4 Hz), theta (4-8 Hz), alpha (8-13 Hz) and mu (11-14 Hz) bands are typically more robust to muscle artifact contamination.

7. Stationary Data Analysis

The starting point of most EEG data analysis is *spectral analysis* to assess statistical properties of amplitude and phase of multiple EEG frequency bands. Even when the final goal of the analysis does not involve spectral analysis, examining the spectrum of the EEG is a useful starting point for evaluating data quality and for communication of more complex methods. The spectrum obtained by applying the Fourier transform to a single EEG epoch or time window provides information about its frequency content. Fourier transform algorithms yield estimates of Fourier coefficients that reflect both the amplitude and phase of the oscillations within one frequency band. Fast Fourier Transforms (FFT) are one class of algorithms that are particularly useful, and a number of important issues in practical FFT analysis are detailed in several texts

(see Bendat & Piersol 2011 for examples). Other Fourier analysis or spectra-like algorithms such as multi-taper analysis (Percival & Walden, 1993), autoregressive models (Ding et al., 2000), wavelet analysis (Lachaux et al. 2002), and Hilbert transforms (Bendat & Piersol 2011; van Quyen et al. 2001; Deng & Srinivasan, 2010) have potential applications in EEG, particularly in the analysis of short epochs characterizing EEG behavior after an experimental stimulus. Any of these algorithms can be used to carry out spectral analysis of time series, but an FFT based analysis provides a quick and easy assessment of the spectrum.

The amplitude spectrum of one epoch of EEG is an exact representation of the frequency content of that particular time window, but only provides one observation about the random process generating the signal. The full ensemble of K epochs $\{V_k(t)\}$ can be used to estimate statistical properties of the random process generating the EEG under the assumption of weak stationarity (Bendat and Piersol, 2011). Weak stationarity is obtained if the mean and variance of the signal do not change with time. This can be verified by obtaining an estimate of mean and variance at each time point across epochs. Typically, the weak stationarity assumption is reasonable in the analysis of spontaneous EEG in resting-state experiments; it is not reasonable in any experiment where a sensory stimulus is presented and/or a motor response is obtained from the subject.

Estimating the *power spectrum* from an ensemble of epochs yields an estimate of the variance of the signal as a function of frequency. This is a particularly useful approach because EEG contains oscillatory activity in distinct frequency bands that are associated with different brain states. First, for each epoch $V_k(t)$, Fourier coefficients $F_k(f_n)$ are obtained by applying a Fourier Transform, perhaps using the FFT. Then the power spectrum may be estimated from the ensemble of observations by summing over K epochs, given in Eq. 4.

$$P(f_n) = \frac{2}{K}\sum_{k=1}^{K} F_k(f_n) F_k^*(f_n) = \frac{2}{K}\sum_{k=1}^{K} \left|F_k(f_n)\right|^2 \qquad n = 1, 2, ..., N/2 - 1 \qquad (4)$$

When applying the FFT, the frequency resolution $\Delta f = 1/T$ of the resulting power spectrum depends inversely on the length of each observation T as $f_n = n/T$ where n

indexes the frequency band. The equation for the power spectrum is multiplied by a factor of two because the Fourier transform provides amplitudes split between positive and negative complementary phases and only amplitudes at positive phases are usually calculated. If the mean value of the signal is zero, the power spectrum summed over all frequencies is equal to the variance in the signal, a relationship known as *Parseval's theorem* (Bendat and Piersol 2011). The square root of the power spectrum, the *amplitude spectrum*, places more emphasis on non-dominant spectral peaks. Any algorithm used to obtain Fourier coefficients can be used to approximate Eq. 4; although the definition of frequency bands depends on the algorithm. Eq. 4 provides a definition of the EEG power spectrum in units that depend on the frequency resolution Δf. In order for the results to be compared across all choices of epoch length, the power spectrum is sometimes normalized by the frequency resolution Δf to express power in units of μV^2 per Hz.

Before the rise of widespread access to computational power and use of the Fast Fourier Transform, the power spectrum of a time series was typically calculated in a two stage procedure. First the *autocorrelation function* was estimated and then the Fourier transform of the autocorrelation function was calculated. The result is equivalent to the power spectrum of the signal. The autocorrelation function is the covariance of the signal with itself as a function of lag:

$$R_{VV}(\tau) = E\left[V(t)V(t-\tau)\right] \qquad (5)$$

Like the power spectrum, the true autocorrelation function is an unknown statistical property of the time series and can only be estimated. In Eq. (5) the lag variable τ is defined over positive and negative values. The autocorrelation function contains exactly the same spectral information as the time series of epoch length T if the domain of τ is [-T/2, T/2]. The Fourier transform of the autocorrelation function is then equal to the power spectrum of the signal (Bendat and Piersol, 2001). However in modern spectral analysis the Fourier transform is usually directly calculated before calculating the power spectrum.

Estimation of the power spectrum involves tradeoffs in frequency resolution, statistical power, and weak stationarity. For example, consider the choices involved in

analyzing a 60 second EEG record. Figure 5 demonstrates power spectra of two EEG channels, one occipital and one frontal, recorded with the subject's eyes closed and at rest. The power spectra were obtained using an epoch length T = 60 seconds (Δf =0 .017 Hz) and no epoch averaging (K = 1 epochs). With this choice, the FFT of the entire record is obtained (exact spectra of the two EEG signals), but no information about the statistical properties of the underlying random process is gained. Note that the power spectrum of the occipital channel **(**Fig. 5a**)** contains two peaks, one below 10 Hz and a larger peak above 10 Hz. The frontal channel (Fig. 5b) shows a larger peak below 10 Hz. By examining the other channels it was found that the two peaks have distinct spatial distributions over the scalp, suggesting they have different source distributions. Each peak is surrounded by power in sidebands (adjacent frequency bins) of the two peak frequencies. *The signals are stochastic processes occupying relatively narrow bands in the frequency spectrum.*

To analyze the 60 sec signal properly, we must decide how to divide the record into epochs to implement Eq. 4. The choice is a compromise between the advantage of good frequency resolution yielded by long epochs (large T and small K) and the statistical power of our estimate gained by using a larger number of epochs (small T and large K). If a frequency resolution of Δf = 0.5 Hz is chosen, the record is segmented into K = 30 epochs of length T = 2 sec. If frequency resolution is reduced to Δf =1 Hz, we divide the record into K = 60 epochs of length T = 1 sec. Figures 5c and 5d show the power spectra of the frontal and occipital channels with Δf = 1 Hz (grey circles) and Δf = 0.5 Hz (black circles). The power spectra at the occipital and frontal channels are both dominated by alpha rhythm oscillations. At the occipital electrode (Fig. 5c) two separate peak frequencies are at 9.5 and 10.5 Hz are evident with Δf = 0.5 Hz, but this separation is not revealed with Δf = 1 Hz, where only a single peak frequency at 10 Hz is evident. Lowering frequency resolution has a similar effect at the frontal channel (Fig. 5d), but since there is very little power at 10.5 Hz, the only clear peak appears at 9 Hz. Thus, by choosing a lower frequency resolution we observe different peak frequencies at the two sites, while choosing higher frequency resolution results in pairs of frequency peaks at both sites but with different magnitudes.

By examining the power spectra for the occipital (Fig. 6a) and frontal sites (Fig. 6b) for individual epochs with Δf = 0.5 Hz, evidence is found for two different oscillations within the alpha band. At the occipital channel, individual epochs display two distinct peaks at 9.5 Hz and 10.5 Hz. The first 15 epochs show a strong response at 10.5 Hz but the later epochs show a stronger response at 9.5 Hz. The dominant frequency in each epoch is summarized in the peak power histograms in Fig. 5c showing that individual epochs displayed peak frequencies at both 9.5 Hz and 10.5 Hz. By contrast, very few epochs have a peak frequency of 10.5 Hz at the frontal site (Fig. 5d); most epochs have peak frequencies either at 9.5 Hz or in the delta band (< 2 Hz). Note that during most epochs with strong delta activity in Fig. 5d the alpha peaks are attenuated.

In the previous example, electrodes at different locations show different magnitudes of two distinct oscillations with center frequencies at 9.5 Hz and 10.5 Hz. The natural next step is to measure correlation between electrode sites to assess spatial statistics of the EEG. This is motivated by the idea that correlation of EEG signals should reflect functional connectivity of the brain. Neurons in distant (and nearby) cortex are connected by axons which form the white-matter beneath the gray-matter consisting more of cell bodies (Nunez, 1995). *Coherence* between two electrodes is a correlation coefficient (squared) that measures the consistency of relative phase between signals in a specific frequency band (and is weakly dependent on large amplitude changes). In EEG signals, coherence mainly reflects the consistency of phase differences across epochs, potentially reflecting axon transmission delays (Nunez and Srinivasan, 2006). Coherence ranges from 0 (indicating random phase differences) to 1 (indicating identical phase differences). Like the Pearson correlation coefficient, coherence is a unknown statistical property whose true value depends on the entire theoretical population of all similar epochs and can only be estimated using the given sample of epochs.

One way to estimate coherence between an electrode pair is to first calculate the *cross spectrum* (Bendat and Piersol, 2011). The cross spectrum, provided in Equation 6, is a measure of the joint spectral properties of two channels (i.e. a measure of the Fourier coefficient *covariance*). Fourier coefficients at a certain frequency f_n at each electrode are multiplied and averaged over K epochs to calculate the cross spectrum.

$$C_{uv}(f_n) = A_{uv}e^{j\phi_{uv}} = \frac{2}{K}\sum_{k=1}^{K} F_{uk}(f_n)F_{vk}^{*}(f_n) \quad n = 1, 2, ..., N/2 - 1 \quad (6)$$

Where F_{vk}^{*} refers to the complex conjugate of the Fourier coefficient at channel *v*. Note that the cross spectrum between a channel and itself (*u* = *v*) is equal to the power spectrum (Eq. 4) and is real valued.

In general, the cross spectrum is complex valued and can be thought of in terms of its magnitude (or cross-power) A_{uv} and phase ϕ_{uv} information. The phase of the cross spectrum is the average phase difference between the two channels. This average phase difference is called the *relative phase*. The magnitude information A_{uv} is analogous to the ordinary covariance between two time series, i.e. the *covariance* across observations between two channels in one frequency band. Coherence at f_n is defined by the squared magnitude of the cross spectrum standardized by the product of the power spectra (which are variances) of each signal

$$\gamma_{uv}^{2}(f_n) = \frac{\left|C_{uv}(f_n)\right|^2}{P_u(f_n)P_v(f_n)} \qquad n = 1, 2, ..., N/2 - 1 \qquad (7)$$

Coherence can be thought of as the fraction of variance at frequency f_n in channel *u* that can be explained by a constant amplitude and phase change (i.e. a *linear transformation* of Fourier coefficients) of the data at frequency f_n obtained at channel *v*.

Coherence between channels is most sensitive to phase differences. For instance, if the phase difference is constant over epochs between channels *u* and *v*, coherence is maximized and is equal to 1. If the relative phase between channels *u* and *v* varies across epochs, coherence will be less than one. Furthermore, if the phase difference is random across all epochs, the coherence estimate will approach zero as the number of epochs (*K*) increases. A coherence of 0.4 in frequency band f_n indicates that at that 40% of the variance at one channel can be explained by a linear transformation of the other channel. However this does not imply that a linear relationship actually *exists*, only that the relationship (or part of the relationship) can be approximated by a linear transformation. If the activity at the two channels is truly related nonlinearly (e.g. have a quadratic

relationship), the coherence would provide information as to how well the nonlinear relationship can be approximated by a linear relationship.

If the goal is to estimate phase synchronization independent of amplitude fluctuations, Fourier coefficients in Equation 7 could be normalized by amplitude to obtain *phase-only* coherence. Phase synchronization can also be evaluated with measures of the relative phase distribution across or within epochs (Tass et al., 1998). On the other hand, one reason to include amplitude as in Eq. 6 and 7 is that coherence measures are weighted in favor of epochs with large amplitudes. Trials with large amplitudes are preferred if large amplitudes are indicative of high signal to noise ratios. If only epoch phase information were used, equal emphasis would be placed on low and high amplitude epochs in estimates of phase synchronization. This would potentially reduce the overall signal-to-noise ratio of the analysis.

Typically the goal of EEG coherence studies is to estimate the *functional connectivity* of the brain. Coherent activity between pairs of electrode sites may be either synchronous (zero phase difference) or asynchronous (constant phase difference). In other words asynchronous coherent signals are essentially "synchronous with a time lag." Figure 7 shows the coherences between an electrode *x* and a ring of electrodes at progressively greater distances from *x*, labeled 1-9. The subject is at rest with eyes closed, a state in which coherence is usually high in the alpha band (Nunez, 1995). The estimated coherence between electrode *x* and electrode *n* is labeled *x:n*. The electrode positions are shown and the distance between adjacent electrodes is about 2.7 cm. At the closest electrode pair *x:1*, coherence is very high (above 0.75) at all frequencies (i.e. coherence is generally independent of temporal frequency). This effect was predicted by the observed effect of volume conduction of current spreading through the head; the effect of volume conduction is to mix the brain signals at each electrode, which correlates them at all frequencies. This theoretical prediction of coherence due to volume conduction suggests that *the main effect of volume conduction is to artificially inflate coherences at short to moderate distances, and that this effect is independent of frequency*.

As the electrode separation is increased, the pair *x:2* shows lower coherences, but at most frequencies coherence is still above 0.4 suggesting a strong component of

coherence that is independent of frequency. A peak is visible in the alpha band at 9.5 Hz, but it is difficult to evaluate this peak, since there is also a broad elevation of coherence. As the sensor separation is further increased (*x:3*) the floor of the coherences reduces further to about 0.2, and a peak becomes more evident in the 18 Hz range. This electrode is about 10 cm away from electrode *x* consistent with model predictions of volume conduction effects on EEG coherence for electrodes separated by less than 10 cm (Srinivasan et al., 1998). For pairs of electrodes involving sites over the temporal lobes, *x:4* and *x:5*, the floor of the coherences approaches zero at most frequencies except for the alpha band where a second peak at 10.5 Hz is visible. At a very long distance (*x:8*) the coherences are again elevated across all frequencies, suggesting a very small volume conduction effect at long distances as also observed in modeling studies (Srinivasan et al., 1998; Srinivasan et al., 2007).

Spatial statistics, like coherence, will always be influenced by volume conduction effects. In the case of coherence, a simple rule of requiring a separation distance of 10 cm or more can be used to minimize volume conduction effects. Another approach is to use the surface Laplacian to spatially high-pass filter the EEG signals, minimizing the effect of volume conduction (Nunez et al., 1994; Srinivasan et al., 1998). And as new methods are deployed to evaluate EEG spatial statistics (e.g. to make inferences about connectivity), more modeling studies are needed to evaluate the impact of volume conduction in order to interpret these new measures.

8. Nonstationary Data Analysis

A stationary time series is a random process whose statistical distribution is invariant over time. A *weakly* stationary time series is one in which the mean, variance, and autocorrelation of the random process are invariant to shifts in the time at which the sample records are obtained. Many EEG analyses assume weak stationarity in order to evaluate EEG in different brain states such as resting with eyes closed or eyes open, during mental calculations, or during different stages of sleep.

However, in many experiments, especially those related to cognitive functions, a stimulus is presented and/or a motor response is elicited and often both. This structure of

events in an experimental trial implies that the EEG time series is nonstationary, as we can reasonably expect that the statistics of the signals will depend on time relative to the events. Clearly the EEG before a stimulus is presented has a different statistical structure than EEG following the stimulus. In fact we are interested in uncovering these differences!

Many experimenters analyze the time-varying mean of EEG data epochs following an experimental stimulus. The mean responses are called *evoked potentials* (EP) or *event related potentials* (ERP). These types of experimental designs are ubiquitous in the cognitive neuroscience literature. Because we may postulate that only the signals relevant to the stimulus to remain after we average many trials of EEG response data, the EP or ERP is calculated as the ensemble mean of observations across epochs. If the subject views the same stimulus (or stimulus category) in all epochs (e.g. separate experimental trials) then we can expect the average EEG signal to approximate the response of ongoing EEG activity to the stimulus, such that the mean of the potential at each electrode varies as a function of time and is given by

$$\mu(t) = \frac{1}{K}\sum_{k=1}^{K} V_k(t) \qquad (8)$$

Note that in order to calculate an evoked response, EEG is averaged across the dimension of epochs, not across the dimension of time.

Figure 8 shows an example of a visual evoked potential, or the time-varying mean at 124 electrodes of a high-density EEG cap, following presentation of a visual stimulus. Much of the ERP literature focuses on the peaks and troughs of this waveform (Fig. 8a) and its relationship to perception and cognition. These are labeled P1, N1, P2, etc, reflecting the direction and order of the peaks (Luck et al., 2000). The inset topographic maps of the potential at the peaks indicate some spatial distribution, although naturally most of the response is over the back of the head, where visual cortex is located. Visual inspections suggests that this signal is an oscillation with a period of about 120 ms, which is confirmed by the wavelet spectrogram (Fig. 8b) at one channel.

Spectral analysis methods as defined in section 7 can be used to evaluate time-varying power and coherence of the EEG signals. The assumption in these analyses is that over narrow windows of time, e.g., 200 ms, the EEG can be considered stationary. This window is then moved over the epoch. A more convenient approach to calculate time-varying power and coherence is to use the complex Morlet wavelet transform to estimate time-varying Fourier coefficents (Lachaux et al., 2002). Two examples of time-varying power calculated using the Morlet wavelet transform are presented in Figures 8b and 9. Fig. 8b shows the *phase-locked* change in alpha power *after* a visual stimulus is presented. In order to calculate phase-locked power, power of the time-average of epochs given in Eq. 8 can be calculated such that K=1 in Eq. 4, which removes all signal that is not phase-locked. Fig. 9 shows a non-phase-locked "desynchronization" (i.e. decrease) in alpha power in electrode C3 (an electrode close to the left motor-cortex) *before* the subject responded with a button press. Power in the alpha band at electrodes over motor cortex are sometimes called the "mu rhythm" to differentiate it from spectral changes in the alpha band not associated with a motor response.

Steady-state evoked potentials (SSEPs) are another type of evoked potential, associated with experimental designs known as "frequency-tagging" (Ding et al., 2006; Deng and Srinivasan, 2010). SSEPs refer to a frequency-tagging paradigm where EEG responses are observed in narrow frequency bands corresponding to the frequencies and harmonics of a stimulus (Regan, 1977). Steady-state responses can be evoked with flickering visual stimuli (steady-state visual evoked potentials; SSVEPs), modulated auditory stimuli (steady-state auditory evoked potentials; SSAEPs), or rhythmic somatosensory stimuli (steady-state somatosensory evoked potentials, SSSEPs). SSEP paradigms are preferred by many neuroscientists due to their large signal to noise ratios, minimizing the problem of artifacts which are typically broadband. SSVEPs, SSAEPs, and SSSEPs have also been shown to track attention (Tiitinen et al., 1993, Morgan et al., 1996, and Giabbiconi et al., 2004). Our group has also shown that SSVEP data can be used to classify video game players versus non-gamers (Krishnan et al., 2013), differentiate individual differences in attention (Ding et al., 2006; Bridwell et al., 2013), and predict individual differences in perceptual decision making (Nunez et al., 2015).

9. Summary

In this chapter we introduce the physical basis of EEG recording and its implications for the type of brain processes observable with EEG. Practical EEG recording poses additional challenges, especially in relation to physiological artifacts such as muscle artifacts. We recommend that EEG analysis begin with spectral analysis methods, which provide a foundation from which more advanced statistical models can be developed and foster better communication with other EEG scientists. Spectral analysis is ubiquitous in the EEG literature in both stationary and non-stationary experimental designs. Finally, in research involving spatial statistics, the effect of volume conduction must be explicitly considered to make meaningful inferences about functional connectivity in the brain.

References

Bell, A. J., & Sejnowski, T. J. An information-maximization approach to blind separation and blind deconvolution. *Neural computation*, *7*(6), 1129-1159. 1995.

Belouchrani A, Abed-Meriam K, Cardoso JF, and Moulines E, A blind source separation technique using second-order statistics. *IEEE Transactions on Signal Processing*. 45:434-444, 1997.

Bendat JS and Piersol AG, *Random Data. Analysis and Measurement Procedures*, Fourth *Edition*. New York: Wiley, 2011.

Bertrand, O., Perrin, F., & Pernier, J. A theoretical justification of the average reference in topographic evoked potential studies. *Electroencephalography and Clinical Neurophysiology/Evoked Potentials Section*, *62*(6), 462-464, 1985.

Baillet, S., & Garnero, L. A Bayesian approach to introducing anatomo-functional priors in the EEG/MEG inverse problem. *Biomedical Engineering, IEEE Transactions on*, *44*(5), 374-385, 1997.

Bridwell, D. A., Hecker, E. A., Serences, J. T., & Srinivasan, R. Individual differences in attention strategies during detection, fine discrimination, and coarse discrimination. *Journal of neurophysiology*, *110*(3), 784-794, 2013.

Buzsáki, G, *Rhythms of the Brain*. New York: Oxford University Press, 2006.

Cardoso JF Blind signal separation: Statistical principles. *Proc IEEE*, 9:2009-2025, 1998.

Delorme, A., & Makeig, S. EEGLAB: an open source toolbox for analysis of single-trial EEG dynamics including independent component analysis. *Journal of neuroscience methods*, *134*(1), 9-21, 2004.

Delorme, A, Sejnowski, T, Makeig, S. Enhanced detection of artifacts in EEG data using higher-order statistics and independent component analysis. *Neuroimage*. 34(4):1443-49, 2007.

Deng, S., Srinivasan, R., Lappas, T. and D'Zmura, M. EEG classification of imagined syllable rhythm using Hilbert spectrum methods. *Journal of neural engineering*, *7*(4), 046006. 2010.

Deng, S. and Srinivasan, R. Semantic and acoustic analysis of speech by functional networks with distinct time scales. *Brain Research*, 1346, 132 - 144. 2010.

Ding, J., Sperling, G. and Srinivasan, R. Attentional modulation of SSVEP power depends on the network tagged by the flicker frequency. Cerebral cortex, 16(7), 1016-1029. 2006.

Ding, M., Bressler, S.L., Yang, W. and Liang, H. Short-window spectral analysis of cortical event-related potentials by adaptive multivariate autoregressive modeling: data preprocessing, model validation, and variability assessment. Biological cybernetics, 83(1), 35-45. 2000.

Fisch, B.J. and Spehlmann, R., Fisch and Spehlmann's EEG primer: basic principles of digital and analog EEG. Elsevier Health Sciences. 1999.

Fitzgibbon, S.P., DeLosAngeles, D., Lewis, T.W., Powers, D.M.W., Grummett, T.S., Whitham, E.M., Ward, L.M., Willoughby, J.O. and Pope, K.J. Automatic determination of EMG-contaminated components and validation of independent component analysis using EEG during pharmacologic paralysis. Clinical Neurophysiology. 2015.

Gratton, G., Coles, M. G., & Donchin, E. A new method for off-line removal of ocular artifact. *Electroencephalography and clinical neurophysiology*, *55*(4), 468-484, 1983.

Giabbiconi, C. M., Dancer, C., Zopf, R., Gruber, T., & Müller, M. M. Selective spatial attention to left or right hand flutter sensation modulates the steady-state somatosensory evoked potential. *Cognitive brain research*, *20*(1), 58-66, 2004.

Hauk, O. Keep it simple: a case for using classical minimum norm estimation in the analysis of EEG and MEG data. *Neuroimage*, *21*(4), 1612-1621, 2004.

Henson, R. N., Flandin, G., Friston, K. J., & Mattout, J. A Parametric Empirical Bayesian framework for fMRI- constrained MEG/EEG source reconstruction. *Human brain mapping*, *31*(10), 1512-1531, 2010.

Hyvärinen, A., & Oja, E. A fast fixed-point algorithm for independent component analysis. *Neural computation*, *9*(7), 1483-1492, 1997.

Jung, T. P., Humphries, C., Lee, T. W., Makeig, S., McKeown, M. J., Iragui, V., & Sejnowski, T. J. Extended ICA removes artifacts from electroencephalographic recordings. *Advances in neural information processing systems*, 894-900, 1998.

Krishnan, L., Kang, A., Sperling, G., & Srinivasan, R. Neural strategies for selective attention distinguish fast-action video game players. *Brain topography*, *26*(1), 83-97, 2013.

Lachaux J. P., Lutz, A., Rudrauf, D., Cosmelli, D., Le Van Quyen, M., Martinerie, J., &Varela, F. Estimating the time-course of coherence between single-trial brain signals: an introduction to wavelet coherence. *Electroencephalography and Clinical Neurophysiology* 32(3):157-74, 2002.

Le Van Quyen, M., Foucher, J., Lachaux, J., Rodriguez, E., Lutz, A., Martinerie, J., Varela, F. J. Comparison of Hilbert transform and wavelet methods for the analysis of neuronal synchrony. *J Neurosci Methods*. 111(2):83-98, 2001.

Lopes da Silva FH and Storm van Leeuwen W, The cortical alpha rhythm in dog: the depth and surface profile of phase. In: MAB Brazier MAB and H Petsche (Eds) *Architectonics of the Cerebral Cortex*. New York: Raven Press, pp 319-333, 1978.

Lopes da Silva, F. H. Dynamics of EEGs as signals of neuronal populations: models and theoretical considerations. In: E Niedermeyer and FH Lopes da Silva (Eds) *Electroencephalography. Basic Principals, Clinical Applications, and Related Fields. Forth Edition*. London: Williams and Wilkins, pp 76-92, 1999.

Luck, S. J., Woodman, G. F., & Vogel, E. K. Event-related potential studies of attention. *Trends in cognitive sciences*, *4*(11), 432-440, 2000.

Makeig, S., Bell, A. J., Jung, T. P., & Sejnowski, T. J. Independent component analysis of electroencephalographic data. *Advances in neural information processing systems*, 145-151, 1996

Makeig S, Debener S, Onton J, & Delorme A, Mining event-related brain dynamics, *Trends in Cognitive Science*, 8(5):204-210, 2004.

McMenamin, B.W., Shackman, A.J., Greischar, L.L. and Davidson, R.J. Electromyogenic artifacts and electroencephalographic inferences revisited. Neuroimage, 54(1), 4-9. 2011.

Morgan, S. T., Hansen, J. C., & Hillyard, S. A. Selective attention to stimulus location modulates the steady-state visual evoked potential. *Proceedings of the National Academy of Sciences*, *93*(10), 4770-4774, 1996.

Mognon, A., Jovicich, J., Bruzzone, L., & Buiatti, M. ADJUST: An automatic EEG artifact detector based on the joint use of spatial and temporal features. *Psychophysiology*, *48*(2), 229-240, 2011.

Murias, M., Swanson, J. M., & Srinivasan, R. Functional connectivity of frontal cortex in healthy and ADHD children reflected in EEG coherence. *Cerebral Cortex*. 17:1788-1799, 2007.

Nunez, M. D., Srinivasan, R., & Vandekerckhove, J. Individual differences in attention influence perceptual decision making. *Frontiers in psychology*, *8*, 2015.

Nunez, P.L. A study of origins of the time dependencies of scalp EEG: I-theoretical basis. Biomedical Engineering, IEEE Transactions on, (3), 271-280, 1981.

Nunez, P. L., Silberstein, R. B., Cadusch, P. J., Wijesinghe, R. S., Westdorp, A. F., & Srinivasan, R. A theoretical and experimental study of high resolution EEG based on

surface Laplacians and cortical imaging. *Electroencephalography and clinical neurophysiology*, *90*(1), 40-57, 1994.

Nunez, P. L. *Neocortical Dynamics and Human EEG Rhythms.* New York: Oxford University Press, 1995.

Nunez, P. L. Toward a quantitative description of large scale neocortical dynamic function and EEG. *Behavioral and Brain Sciences* 23: 371-398 (target article), 2000a.

Nunez, P. L. Neocortical dynamic theory should be as simple as possible, but not simpler. *Behavioral and Brain Sciences* 23: 415-437 (response to commentary by 18 neuroscientists), 2000b.

Nunez, P. L. & Srinivasan, R. *Electric Fields of the Brain: The Neurophysics of EEG, 2nd Edition.* New York: Oxford University Press, 2006.

Olbrich, S., Jödicke, J., Sander, C., Himmerich, H. and Hegerl, U.. ICA-based muscle artefact correction of EEG data: What is muscle and what is brain?: Comment on McMenamin et al. Neuroimage, 54(1), 1-3. 2011.

Oostenveld, R., & Praamstra, P. The five percent electrode system for high-resolution EEG and ERP measurements. *Clinical neurophysiology*, *112*(4), 713-719, 2001.

Percival, D. B. & Walden, A. T., *Spectral Analysis for Physical Applications: Multitaper and Conventional Univariate Techniques*, Cambridge U Press, Cambridge, UK, 1993.

Petsche, H. & Etlinger, S. C. *EEG and Thinking. Power and Coherence Analysis of Cognitive Processes.* Vienna: Austrian Academy of Sciences, 1998.

Pfurtscheller, G. & Lopes da Silva, F. H. Event-related EEG/MEG synchronization and desynchronization: Basic principles. *Electroencephalography and Clinical Neurophysiology* 110: 1842-1857, 1999.

Phillips, C., Rugg, M. D., & Friston, K. J. Anatomically informed basis functions for EEG source localization: combining functional and anatomical constraints. *NeuroImage*, *16*(3), 678-695, 2002.

Polich, J., & Kok, A. Cognitive and biological determinants of P300: an integrative review. *Biological psychology*, *41*(2), 103-146, 1995.

Pope, K. J., Fitzgibbon, S. P., Lewis, T. W., Whitham, E. M., & Willoughby, J. O. Relation of gamma oscillations in scalp recordings to muscular activity. *Brain topography*, *22*(1), 13-17, 2009.

Regan, D. Steady-state evoked potentials. *JOSA*, *67*(11), 1475-1489, 1977

Schlögl, A., Keinrath, C., Zimmermann, D., Scherer, R., Leeb, R., & Pfurtscheller, G. (2007). A fully automated correction method of EOG artifacts in EEG recordings. *Clinical neurophysiology*, *118*(1), 98-104.

Shackman, A. J., McMenamin, B. W., Slagter, H. A., Maxwell, J. S., Greischar, L. L., & Davidson, R. J. Electromyogenic artifacts and electroencephalographic inferences. *Brain topography*, *22*(1), 7-12, 2009.

Srinivasan, R., and Deng, S. Multivariate spectral analysis of the electroencephalogram: power, coherence, and second-order blind identification. 2012

Srinivasan, R., Nunez, P.L., Tucker, D.M., Silberstein, R.B., and Cadusch, P.J. Spatial sampling and filtering of EEG with spline Laplacians to estimate cortical potentials. *Brain Topography*, 8:355 366, 1996.

Srinivasan, R., Nunez, P.L., and Silberstein, R.B. Spatial filtering and neocortical dynamics: estimates of EEG coherence. *IEEE Transactions on Biomedical Engineering*, 45:814 826, 1998.

Srinivasan, R. Anatomical constraints on source models for high-resolution EEG and MEG derived from MRI. *TCRT* 5:389-399, 2006.

Srinivasan, R., Winter, W. R., Ding, J., Nunez, P.L., EEG and MEG coherence: Measures of functional connectivity at distinct spatial scales of neocortical dynamics. *Journal of Neuroscience Methods* 166:41-52., 2007.

Tang, A. C., Sutherland, M. T., McKinney, C. J., Validation of SOBI components from high-density EEG, *NeuroImage*, 25:539-553, 2004.

Tass, P., Rosenblum, M. G., Weule, J., Kurths, J., Pikovsky, A., Volkmann, J., Schnitzler, A. & Freund, H. J. Detection of n: m phase locking from noisy data: application to magnetoencephalography. *Physical review letters*, *81*(15), 3291, 1998.

Tiitinen, H., Sinkkonen, J., Reinikainen, K., Alho, K., Lavikainen, J., and Näätänen, R. Selective attention enhances the auditory 40-Hz transient response in humans. *Nature*, *364*(6432), 59-60, 1993.

Tucker, D. M. Spatial sampling of head electrical fields: the geodesic sensor net. *Electroencephalography and clinical neurophysiology*, *87*(3), 154-163, 1993.

Wipf, D., & Nagarajan, S. A unified Bayesian framework for MEG/EEG source imaging. *Neuroimage*, *44*(3), 947-966, 2009.

Whitham, E. M., Pope, K. J., Fitzgibbon, S.P., Lewis, T., Clark, C. R., Loveless, S., Broberg, M., Wallace, A., DeLosAngeles, D., Lillie, P., Hardy, A., Fronsko, R.,

Pulbrook, A. and Willoughby, J. O., Scalp electrical recording during paralysis: quantitative evidence that EEG frequencies above 20Hz are contaminated by EMG. *Clinical Neurophysiology*, 118(8): 1877-1888, 2007.

Whitham, E. M., Lewis, T., Pope, K. J., Fitzgibbon, S. P., Clark, C. R., Loveless, S., DeLosAngeles, D., Wallace, A. K., Broberg, M., and Willoughby, J. O. Thinking activates EMG in scalp electrical recordings. *Clinical neurophysiology: official journal of the International Federation of Clinical Neurophysiology*, *119*(5), 1166, 2008.

Wu, J., Quinlan, E. B., Dodakian, L., McKenzie, A., Kathuria, N., Zhou, R. J., Augsburger, R., See, J., Le, V. H., Srinivasan, R., and Cramer, S. C. Connectivity measures are robust biomarkers of cortical function and plasticity after stroke. *Brain*, *138*(8), 2359-2369, 2015.

Yuval-Greenberg, S., Tomer, O., Keren, A. S., Nelken, I., and Deouell, L. Y. Transient induced gamma-band response in EEG as a manifestation of miniature saccades. *Neuron*. 58(3): 429-441, 2008.

Ziehe, A., Laskov, P., Muller, K.R., Nolte, G. A linear least-squares algorithm for joint diagonalization. *Proceedings ICA2003,* 469–474. 2003.

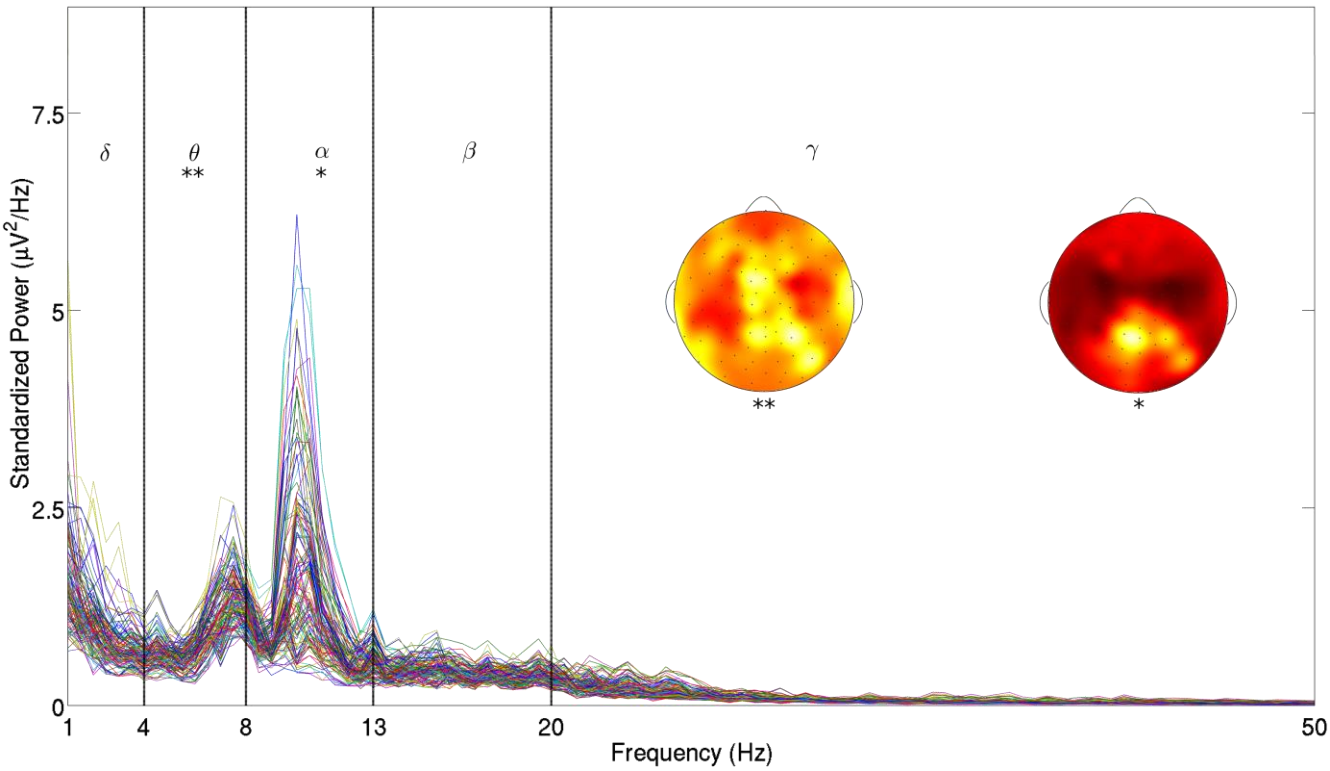

Figure 1. Typical power spectra of 124 EEG channels of 66 seconds (epoch length T = 2 sec with K = 33 epochs) of data from a subject (male, 25 yrs) who fixated on a computer monitor with his eyes open. While EEG spectral band definitions vary from lab to lab and across different fields, bands are typically defined as follows: delta 1-4 Hz, theta 4-8 Hz, alpha 8-13 Hz, beta 13-20 Hz, and gamma > 20 Hz. Some groups also identify the mu rhythm which exists as a peak either in the alpha or beta bands and typically has high power over the motor cortex. In the eyes-open resting data, with some artifact power removed using Independent Component Analysis (ICA), we see peaks in the delta, theta, and alpha bands and some power in the beta band. However the dominant peaks in the spontaneous EEG are in the theta and alpha bands, which have different spatial distributions over the electrodes and are associated with different cognitive functions. Topographic scalp maps were generated by summing power across frequencies in the theta (left) and alpha (right) frequency bands and interpolating between electrodes, such that brighter values correspond to higher power. Alpha, which is empirically associated with the resting state, has maximum power over parietal channels as indicated by the right topographic scalp map.

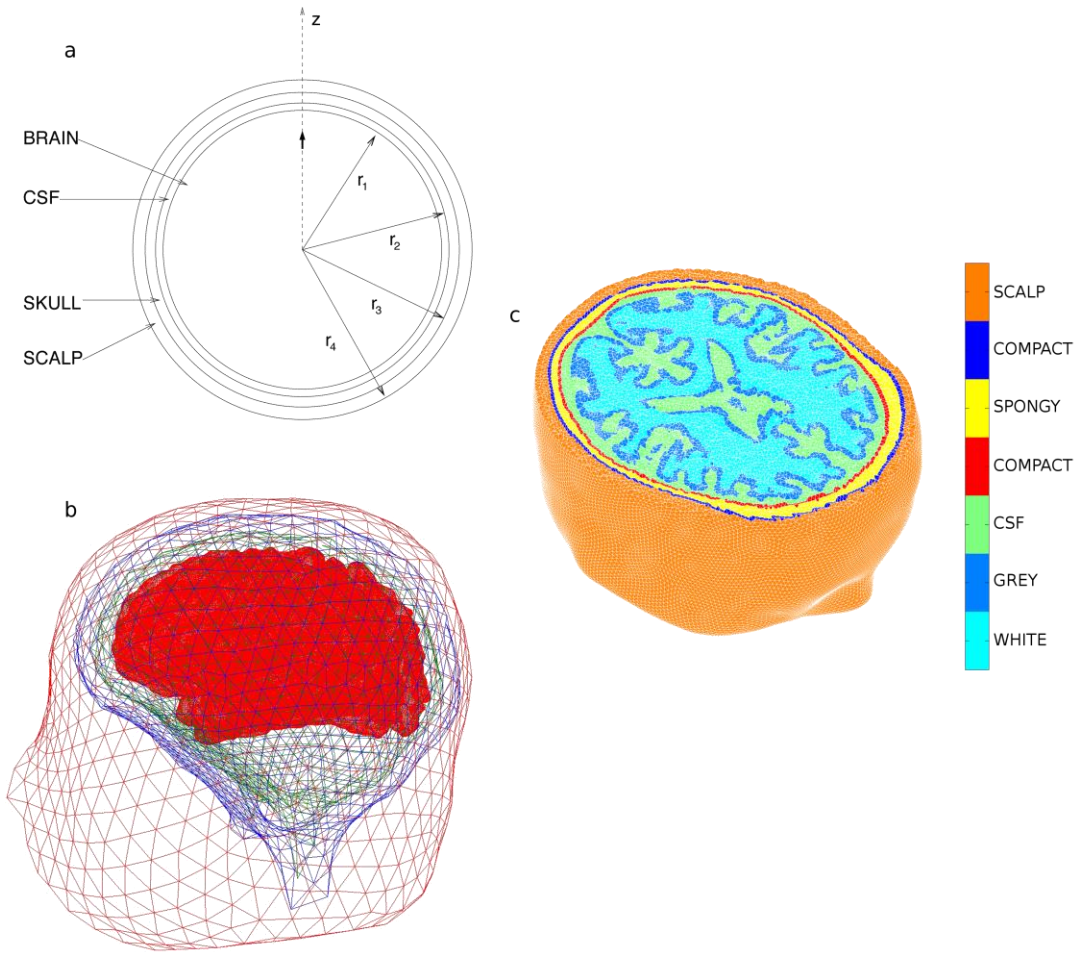

Figure 2. Volume conduction models for EEG. (*a*) A dipole is shown in the inner sphere of a *4-concentric spheres head model* consisting of the inner sphere (brain) and three spherical shells representing CSF (cerebral spinal fluid), skull and scalp. The parameters of model are the radii (r_1, r_2, r_3, r_4) of each shell and the conductivity ratios (σ_1/σ_2, σ_1/σ_3, σ_1/σ_4). Typical values are: radii (8, 8.1, 8.6, 9.2 cm) and conductivity ratios (0.2, 40, 1). This model is used in the simulations in this chapter. (*b*) A realistic shaped boundary element model (BEM) of the head. The brain and scalp boundaries were found by segmenting the images with a threshold, and opening and closing operation respectively, while the outer skull boundary was obtained by dilation of the brain boundary (ASA, Netherlands). Although geometrically more accurate than the spherical

model, the (geometrically) realistic BEM may be no more accurate than a concentric spheres model because tissue resistivities are poorly known. (*c*) A realistic finite element model (FEM) obtained from MRI. This model has potentially better accuracy than the BEM model because the skull is subdivided into three layers corresponding to hard (compact) and spongy (cancellous) bone layers.

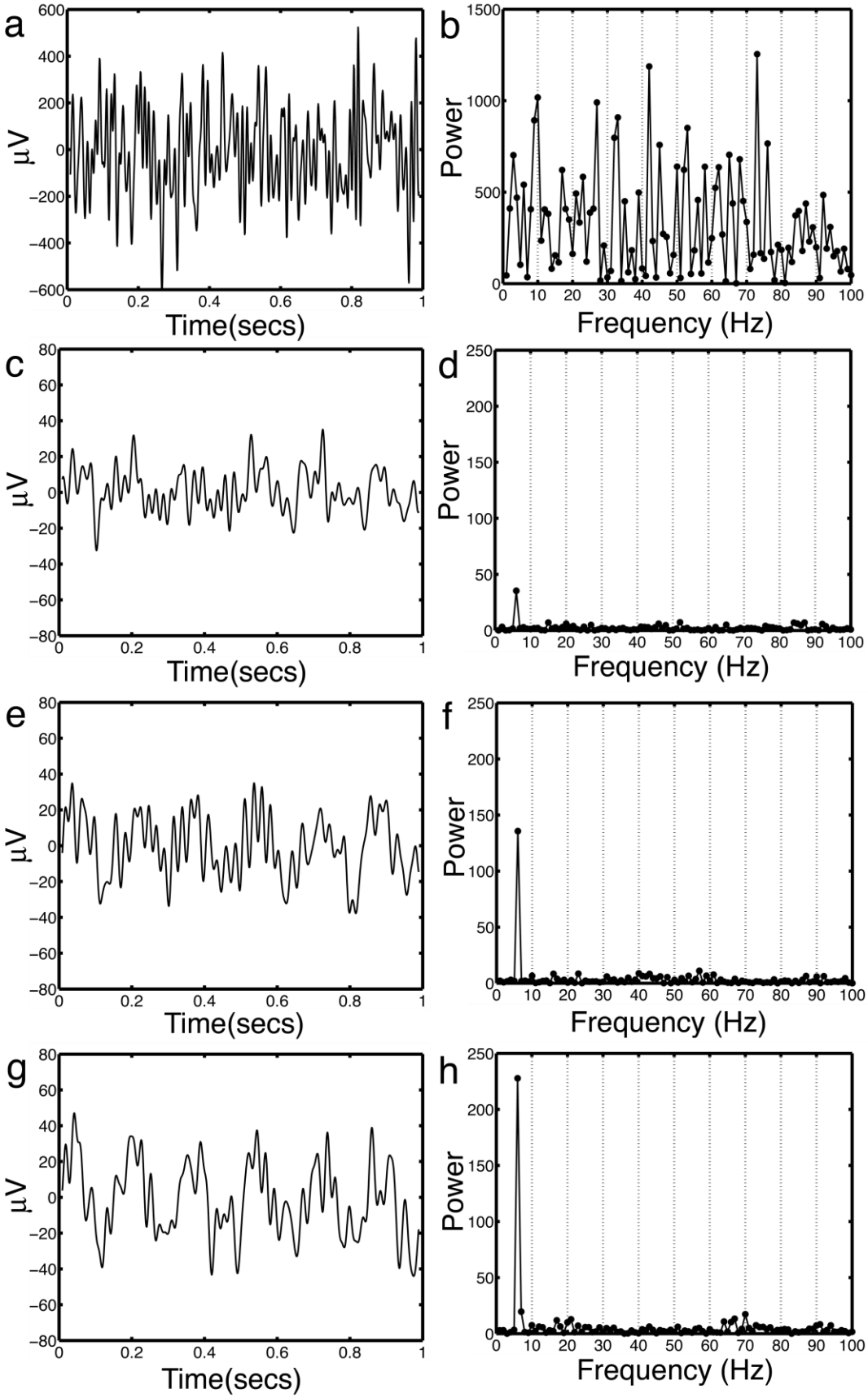

Figure 3. (*a*) Time series of a dipole meso-source **P**(**r**, *t*) composed of a 6 Hz, 15 μV

sine wave added to Gaussian random noise with a standard deviation of $\sigma = 150$ μV. The Gaussian random noise was low pass filtered at 100 Hz. The sine wave has variance (power) equal 1% of the noise. (*b*) Power spectrum of the time series shown in Part (a). The power spectrum has substantial power at many frequencies other than 6 Hz. (*c*) Time series recorded by an electrode on the outer sphere (scalp) of a four concentric spheres model above the center of a dipole layer of diameter 3 cm. The dipole layer is composed of 32 dipole sources $\mathbf{P}(\mathbf{r}, t)$ with time series constructed similar to Part (a) with independent Gaussian noise (uncorrelated) at each dipole source. Scalp potential was calculated for a dipole layer at a radius r_z = 7.8 cm in a four concentric spheres model. The model parameters were radii (r_1, r_2, r_3, r_4) = (8, 8.1, 8.6, 9.2) and conductivity ratios $(\sigma_1/\sigma_2, \sigma_1/\sigma_3, \sigma_1/\sigma_4)$ = (0.2, 40, 1). Notice that the time series is smoother than in the case of the individual dipole source. (*d*) Power spectrum of the time series shown in Part (c). Note the peak at 6 Hz. (*e*) Time series similar to Part (c), but due to a dipole layer of diameter of 4 cm composed of 68 dipole sources. (*f*) Power spectrum of the time series shown in Part (e). (g) Similar time series to Part (c), but with a dipole layer of diameter 5 cm composed of 112 dipole sources. The presence of the 6 Hz sinusoid is obvious from the time series. (*h*) Power spectrum of the time series shown in Part (g). A large spectral peak at 6 Hz is evident.

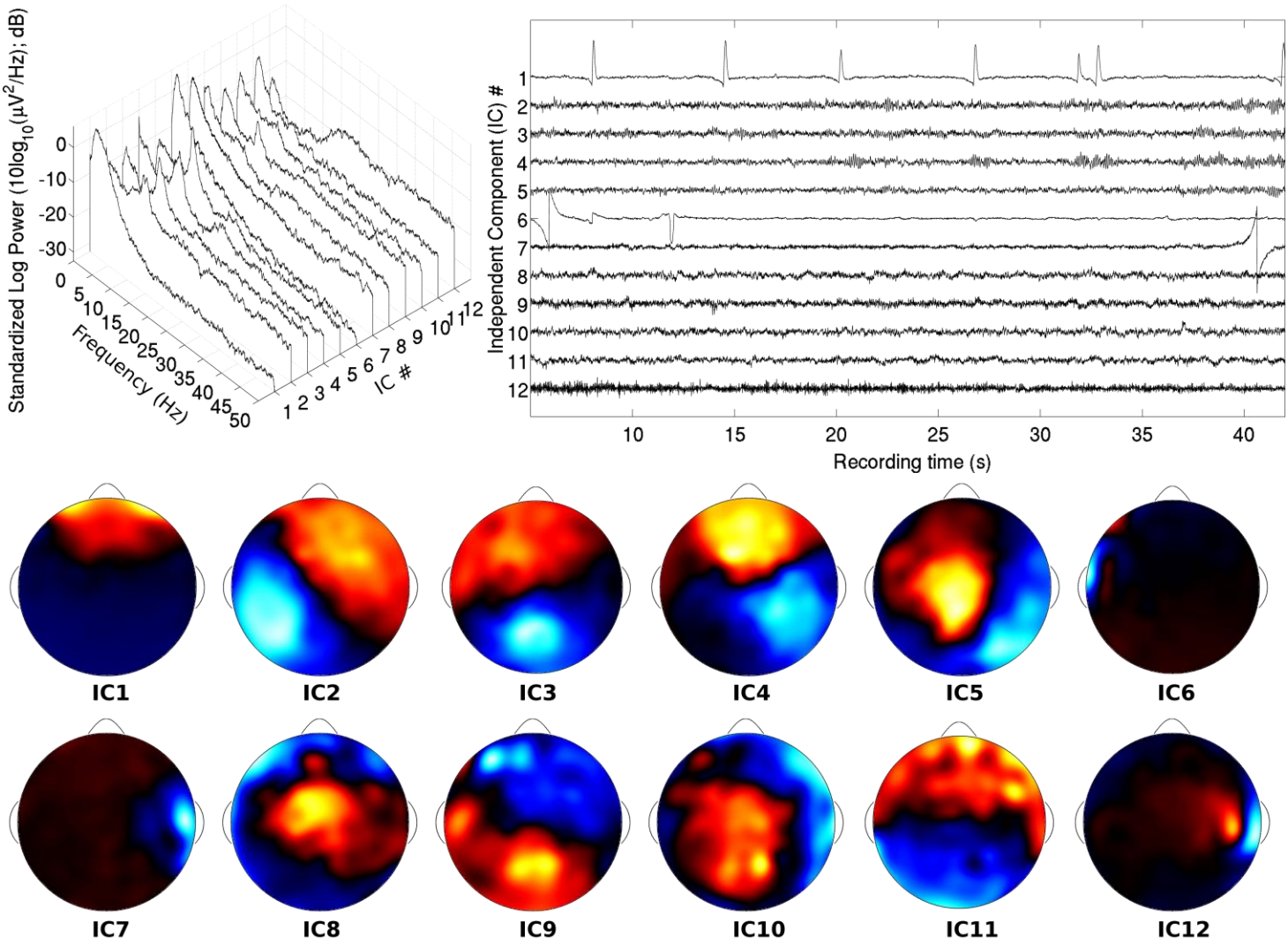

Figure 4. (From top-left, clockwise) Power spectra, time courses, and spatial loading topographies of the first twelve independent components (ICs) from an Independent Component Analysis (ICA) of an EEG recording while a subject (male, 25 yrs) was fixating on a computer monitor. The ICs are ordered by their contribution to the total variance in the raw data. ICs that are likely to reflect artifact contribution can be removed from the raw EEG data. IC1 is indicative of an eye blink. IC6 and IC7 are indicative of temporary electrical discontinuities. IC12 is indicative of muscle artifact.

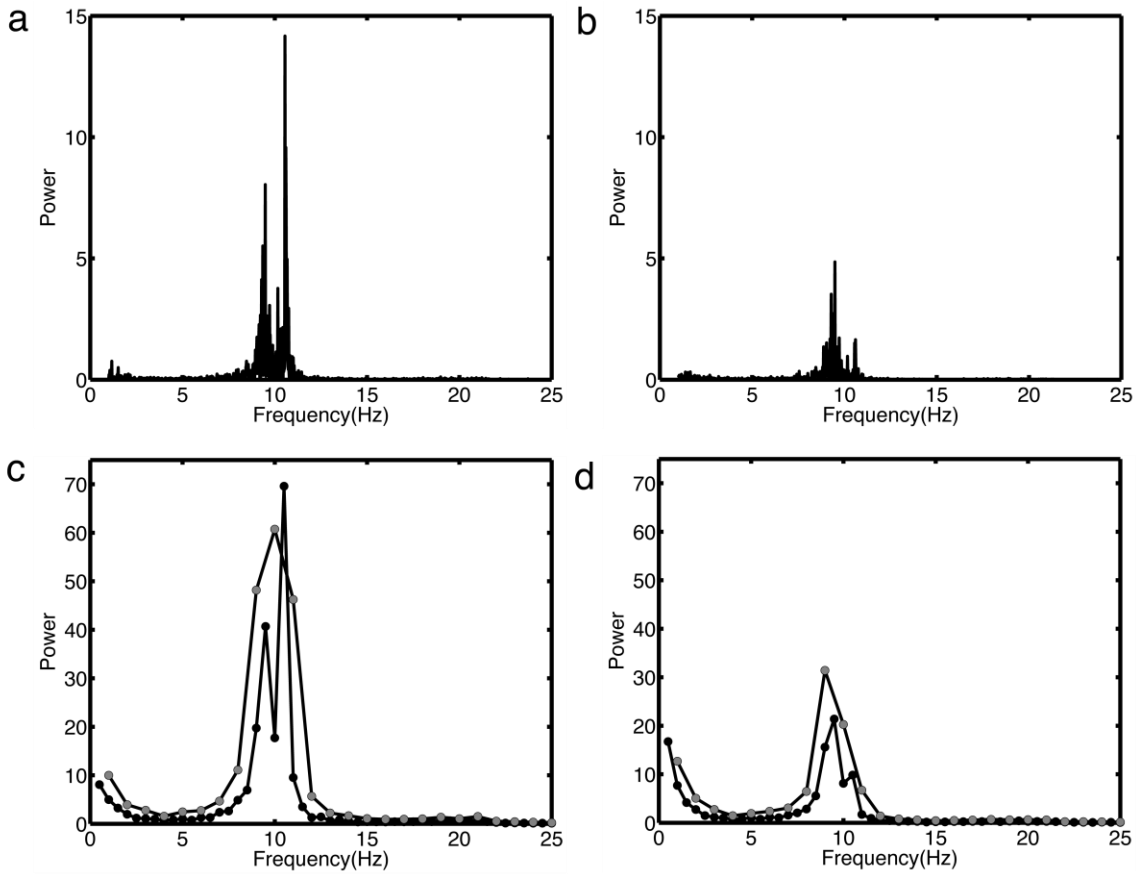

Figure 5. Example power spectra from a single subject (female, 22 yrs). The subject is at rest with eyes closed. (*a*) Power spectrum of a midline occipital channel with epoch length T = 60 sec and K = 1 epochs. The power spectrum appears to have two distinct peaks one below 10 Hz and one above 10 Hz. (*b*) Power spectrum at a midline frontal channel with epoch length T = 60 sec and K = 1 epochs. Here only the peak below 10 Hz is visible. (*c*) Power spectra of a midline occipital channel calculated with two different choices of epoch length T and number of epochs K. The grey circles indicate the power spectrum with T = 1 sec and K = 60 epochs. The black circles indicate the power spectrum with T = 2 sec and K = 30 epochs. (*d*) Power spectra of a midline frontal channel calculated as in Part (c).

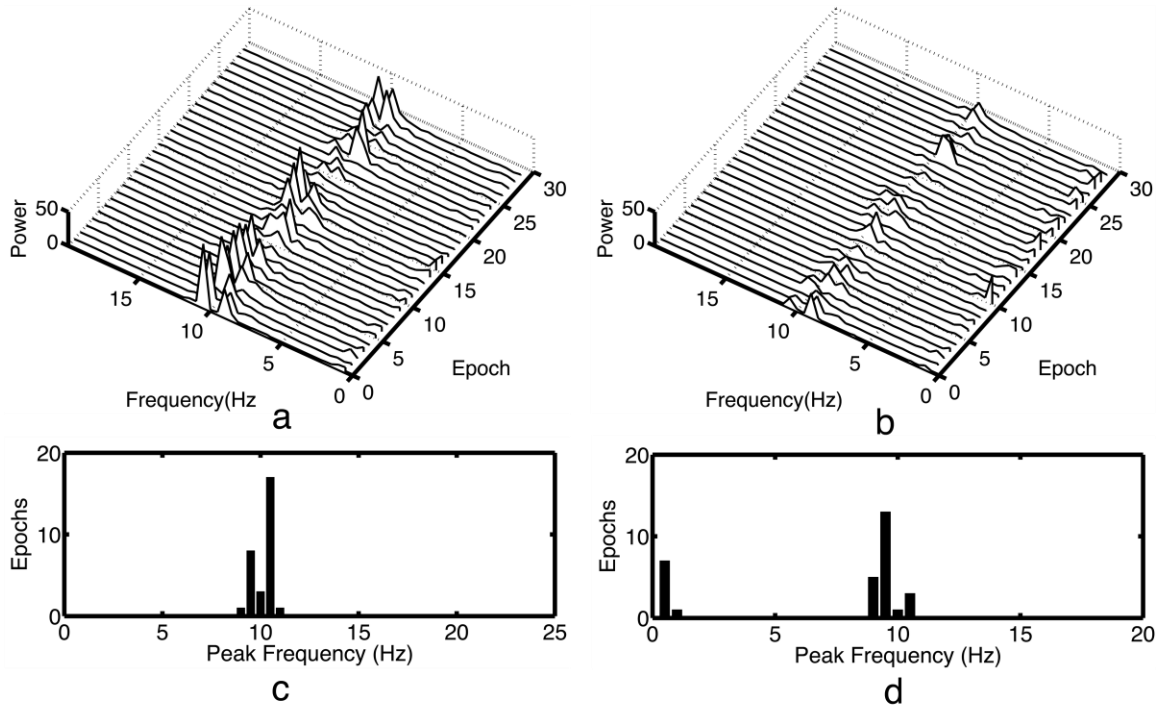

Figure 6. (*a*) Plots of 30 (individual epoch) power spectra for the occipital channel shown in Figs. 5a and 5c. (*b*) Plots of the same 30 individual epoch spectra for the frontal channel shown in Figs. 5b and 5d. (*c*) Peak power histograms show the distribution of peak frequencies for the 30 epochs shown in Part (a). (*d*) Peak power histograms for the 30 epochs shown in Part (b).

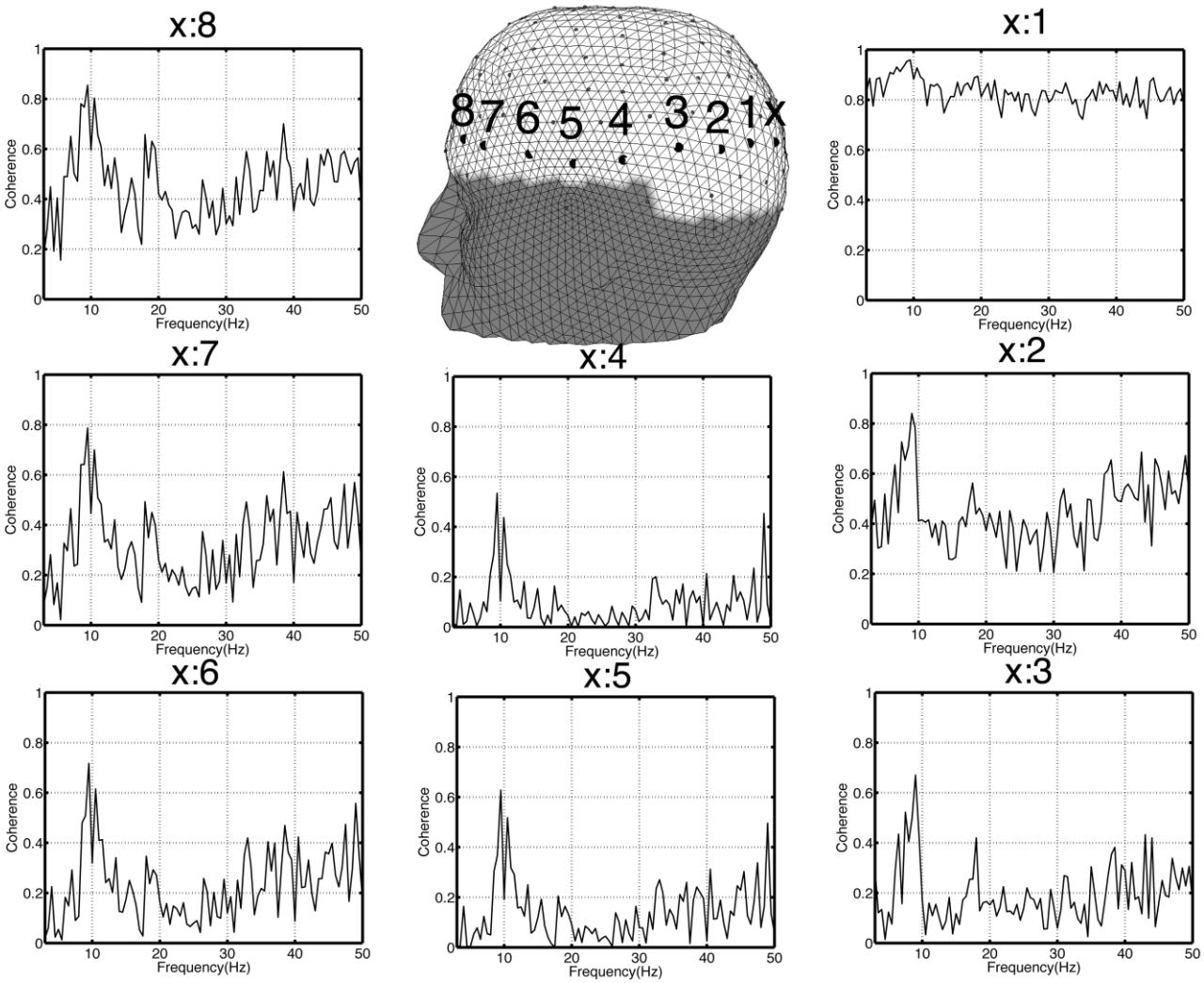

Figure 7. Scalp potential coherence spectra from a subject (female, 22 yrs) at rest with eyes closed in order to maximize alpha coherence. Coherence was estimated with T = 2 sec (Δf = 0.5 Hz) in a 60 sec record. The head plot shows the location of 9 electrodes, labeled x and 1 through 8. Coherence spectra between electrode x and each of the other electrodes 1-8 are shown, with increasing separations along the scalp. Note that very close electrodes have higher coherence independent of frequency as predicted by the theoretical volume conductor model. Alpha band coherence is high for large electrode separations, apparently reflecting the large cortical source coherence.

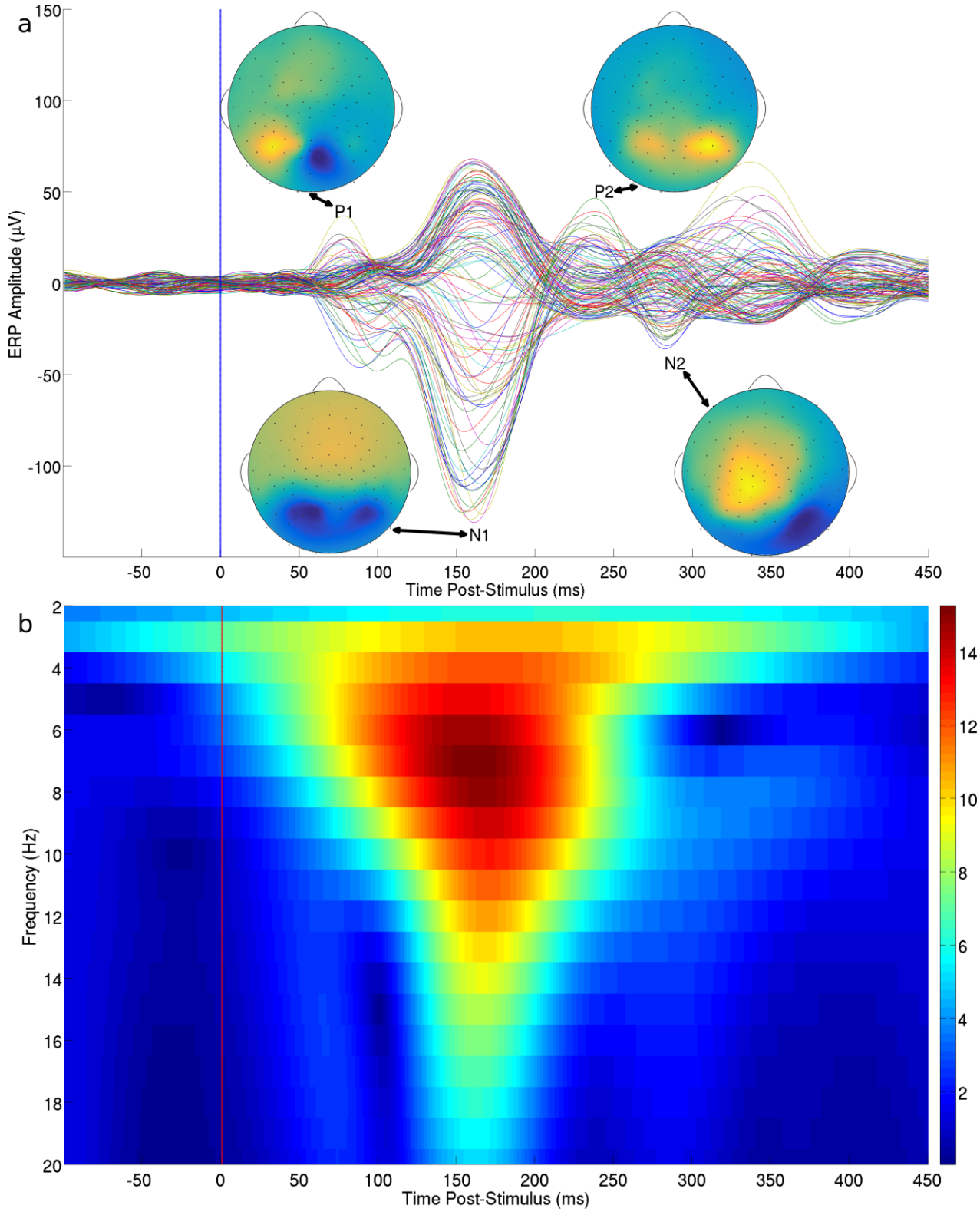
a
ERP Amplitude (μV)
150
100
50
0
-50
-100
P1
P2
N1
N2
-50
0
50
100
150
200
250
300
350
400
450
Time Post-Stimulus (ms)
b
Frequency (Hz)
2
4
6
8
10
12
14
16
18
20
14
12
10
8
6
4
2
-50
0
50
100
150
200
250
300
350
400
450
Time Post-Stimulus (ms)

Figure 8. (*a*) A typical Visual Evoked Response (VEP; also known as an Event Related Potential; ERP) to a large, high contrast sinusoidal grating stimulus recorded at 124 electrodes of a high-density 128 Electrical Geodesics, Inc. (EGI) cap. The VEP was calculated by averaging low-pass Butterworth filtered data (with a 20 Hz passband) across all trials in one subject (male, 23 yrs) and by subtracting each trial by the time average of 200 milliseconds before that trial's stimulus onset (to *baseline* the VEP). Topographies of traditional local peaks (Luck et al., 2000) are labeled with *P1*, *N1*, *P2*, and *N2* indicating the first and second positive and negative peaks over posterior electrodes. The N1 and P2 components evoke typical bilateral responses over parietal electrodes. The P1 and N2 reflect other network behavior related to processing of the visual stimulus. (*b*) A time-varying, phase-locked power spectrum of the same average data at an electrode over the left parietal cortex calculated with a Morlet wavelet transform. As shown by the wavelet, the VEP can also be thought of as a phase-locked alpha response to the visual stimulus.

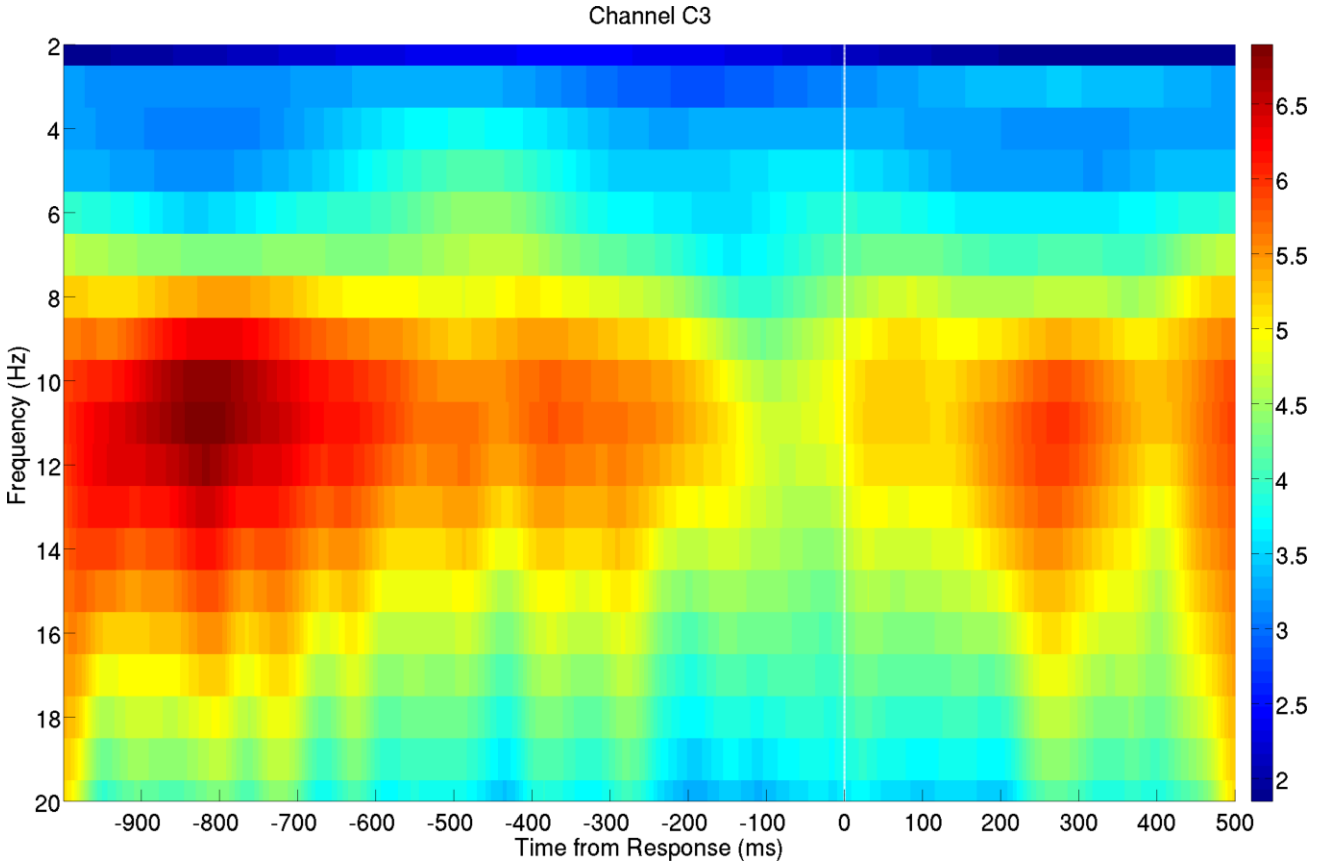

Figure 9. A *non-phase-locked* time-varying power spectrum from the same subject and visual task as in Fig. 8 such that power was calculated using all K=157 epochs time-locked to the motor response (button press given by the right or left hand). Data from a left-central electrode C3 in the 10-20 electrode placement system is presented. Mu power *"desynchronizes"* (i.e. decreases) approximately 200 ms before the button press, likely reflecting cognitive control over the motor response. Similar magnitude of mu power before the desynchronization is observed after the motor response.

@InCollection{Nunez2016b,
 author = {Nunez, Michael D. and Nunez, Paul L. and Srinivasan, Ramesh},
 title = {Electroencephalography ({EEG}): neurophysics, experimental methods, and signal processing},
 booktitle = {Handbook of Neuroimaging Data Analysis},
 year = {2016},
 editor = {Ombao, Hernando and Linquist, Martin and Thompson, Wesley and Aston, John},
 volumes = {Advance online publication},
 publisher = {Chapman \& Hall/CRC},
 isbn = {9781482220971},
 pages = {175--197},
 doi = {10.13140/rg.2.2.12706.63687},
 url = {http://www.researchgate.net/publication/290449135_Electroencephalography_EEG_neurophysics_experimental_methods_and_signal_processing},
}